2026 IEEE International Conference on Robotics and Automation (ICRA 2026)
June 1-5, 2026. Vienna, Austria

Step Placement Swing Control for Powered Knee-Ankle Prostheses

Michael Feldkamp and Rachel Gehlhar Humann

***Abstract*— Humans engage in alternating locomotion patterns in daily life by continuously adjusting step placement. Step placement control in powered prostheses could benefit prosthesis users by supporting speed-adaptation and improving gait stability. This paper uses a data-driven predictive step placement model and a task-space swing controller to achieve human-like step placement patterns on a powered prosthesis platform in simulation. We designed the predictive model to estimate future desired step placement from current user-prosthesis states by analyzing biological gait patterns from a motion-capture dataset. We also present a novel 3D human-prosthesis simulation for evaluating prosthesis controllers with inputs from human walking experiments. In this simulation, we demonstrate our step placement controller with 22 subject models, each with 28 steady-state and 35 non-steady-state walking conditions. Simulation results show that this speed-adaptive control framework achieves human-like step placement and Margin of Stability patterns with respect to walking speed.**

I. Introduction

The prevalence of major lower-limb amputation in the United States is currently 1.1 million, and is projected to increase by 145% by the year 2060 [1]. Prosthetic legs aim to replace the function of the lost limb and assist the user in various tasks. Humans engage in alternating locomotion patterns in daily life, such as walking at different speeds in short bouts [2], climbing stairs or inclines, turning, and running. Step placement, the position of the leading foot at heel strike, is constantly regulated to achieve these locomotion patterns. For example, changing step placement and cadence directly facilitates changes in walking speed [3], while adjusting step placement can restore and maintain walking stability in the face of variations in terrain [4], inclines [5], tripping hazards [6], and external perturbations [7], [8]. However, the inability for current commercial prostheses to actively modulate step placement presents a challenge for lower-limb prosthesis users. To achieve correct step placement during walking, prosthesis users often compensate with asymmetric changes in joint motion [9], which are associated with residual joint injury and muscle overuse [10], [11].

Unlike commercial passive prostheses, powered prostheses can intelligently adjust their assistance in response to their user's motion to enable various locomotion modes, improve balance, and reduce user compensation [12]. Adaptive gait control is often implemented in lower limb prostheses by modulating pre-defined joint-level trajectories [13]–[15], impedance control parameters [16], or modeling muscle dynamics [17], [18] to replicate human biomechanics at different walking speeds. Controllers focused on swing phase rely on joint trajectory planning [19], [20], sometimes specifically for trip avoidance [21]. These methods aim to reproduce joint-level motions across walking speeds, but they rely on independent controllers for each joint, without accounting for how they influence step placement overall. Task-space control allows regulation of system-level objectives [22], and could provide a framework to coordinate multi-joint prostheses with a unified objective to achieve human-like step placement patterns.

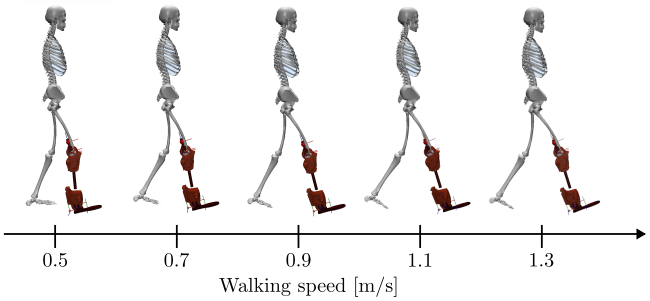

Fig. 1. Knee-ankle prosthesis demonstrating human-like step placement patterns in human-prosthesis simulation across a range of walking speeds.

Since human walking involves controlled forward falling, step placement is an important method of controlling the body's motion through space [23], [24]. Step placement specifically modulates ground reaction force (GRF) magnitudes and directions to stabilize the body's center of mass (CoM) [25]. Indeed, step placement is strongly linked to the position and velocity of the pelvis or CoM prior to heel strike [26] to the degree that simple mechanical walking models, such as an inverted pendulum, effectively predict and imitate human gait [27], [28]. Many accepted walking stability metrics, most notably the Margin of Stability (MoS) [29], are based on quantifying the effects of foot positions on the CoM motion [27], [30], [31].

Bipedal gait is often modeled by an inverted pendulum, which focuses on the relationships between the feet and the CoM. Bipedal robotics control researchers have used the step placement-CoM relationship to develop methods for stable gait generation and control [32]. Full control over all robot joints and real-time measurements of the CoM allow the implementation of accurate CoM-based step placement control. By contrast, this type of control cannot be directly applied to prostheses since the user's joints and CoM cannot be measured without requiring the user to wear

*This material is based upon work supported by the Minnesota Robotics Institute 2025 Seed Grant and the National Science Foundation Graduate Research Fellowship Program under Grant No. 2237827. Any opinions, findings, and conclusions or recommendations expressed in this material are those of the author(s) and do not necessarily reflect the views of the National Science Foundation.

M. Feldkamp and R.G. Humann are with the Department of Mechanical Engineering, University of Minnesota, Minneapolis, MN 55455 USA. Emails: {feldk066, rghumann}@umn.edu

a cumbersome number of sensors, nor does the prosthesis have full control over the human-prosthesis CoM.

Another challenge in developing speed-adaptive prosthesis controls is a realistic simulation environment in which to assess controller performance with human inputs at different walking speeds. However, prior work on such simulators is scarce and typically involves simplifying the human-prosthesis system. The work of [33] optimized swing control parameters with a 1 DOF prosthetic leg simulation, but did not include human inputs at the socket. The work of [34] forward-simulated the human-prosthesis system, but prescribed the human motion based on optimized bipedal robot dynamics. Similar work in [35] replayed human-prosthesis motion capture data to calculate femur-socket interaction forces for a single walking speed. Unlike these approaches to prosthesis simulators, a speed-adaptive controller must be tested with human inputs derived from the natural step-to-step variations and speed changes seen in human walking.

Here, we address these challenges to develop a speed-adaptive step placement controller and a novel human-prosthesis simulation environment. Section II describes our design of a predictive step placement model motivated by human gait biomechanics and related work in bipedal robots. This section also covers the development of a model-based task-space controller for a knee-ankle prosthesis. In Section III, we describe the simulation environment and our use of human gait motion-capture recordings to realistically simulate prosthesis motion. Section IV details extensive simulation tests of our realized step placement controller, and assesses its performance in the context of the MoS. Lastly, we discuss our conclusions and future work in Section V.

II. Step Placement Control

The design of our step placement controller is inspired by human gait models and their applications in bipedal robots. We construct user-specific step placement models to predict desired step placement from user states during stance phases. We modulate human-like trajectories and design a task-space controller to achieve this placement with a prosthesis.

A. Step Placement in Humans and Bipedal Robots

Prior work on bipedal robot control has used the inverted pendulum as a model of bipedal gait to plan future step placement from current CoM states. The recent work of [32] generated and realized stable gait on a Cassie robot using a hybrid variation of the linear inverted pendulum model (H-LIP) as the basis for consistent step planning. Specifically, the H-LIP model defined the "step-to-step" (S2S) dynamics: how the CoM state and step length of the current step relate to the CoM state of the next step. A high-level controller could then reduce CoM state error by adjusting the next step length through feedback control. During swing phase, this was realized by controlling the relative motions of the swing leg and CoM. To better capture the true nonlinear S2S dynamics, such as the inertia of the swinging leg, [36] designed a data-driven model to directly learn the S2S dynamics from walking robot data. This approach enabled the authors to develop robust walking control capable of external push recovery. Although directly adapting this approach to prosthesis step placement control is appealing, two main limitations prevent this: first, the prosthesis cannot measure the relative positions of the sound leg and CoM, especially during swing phase; second, the optimal human CoM states to stabilize via feedback control are unknown.

B. Predictive Step Placement Model

To achieve speed-adaptive step placement control, we first determine where and when the prosthesis foot should land at the end of swing phase. Given a relationship exists between human COM states and future step placement [26], we seek to predict desired step placement from a prosthesis user's current state. Since most variations in states and step placement are due to changes in walking speed, we aim to capture this relationship across a range of speeds.

Note. Step placement in the sagittal plane is a function of the hip, knee, and ankle of both legs. A knee-ankle prosthesis can only affect the prosthesis-side's hip-to-heel step length through the contributions of the knee and ankle. Our analysis of hip-heel positions revealed that knee and ankle configuration at heel strike plays an important role in step placement. First, we found that the sagittal plane horizontal and vertical hip-heel positions at heel strike varied considerably. These quantities are shown in Fig. 2b for one subject [37]. While this could be due to only varying swing hip flexion, we also computed the heel-knee positions at heel strike in a frame oriented with the femur. This removed the effects of the hip angle on step placement, and showed that these also considerably change with walking speed (Fig. 2b). Comparable distributions of hip and knee angles at heel strike confirm that the knee has a notable influence on step placement with respect to walking speed (Fig. 2c).

The limited sensing information available on-board a prosthesis does not allow measurements of the user's CoM or their foot positions, preventing using these user states as inputs in our step placement predictor. However, the relative distance between the user's prosthesis-side hip and prosthesis foot can be determined. Given the position of a human's hip is close to their CoM, we hypothesized we could also find a relationship between the position of their hip and their foot placement relative to the hip. We therefore formulated a step placement model that uses the relative prosthesis foot-to-hip distance in prosthesis stance as an input to predict the future desired foot position and swing duration.

We employed a data-driven approach inspired by [36] using data from able-bodied walking subjects to create the predictive step placement model. Human motion-capture walking data was sourced from the EPIC Lab dataset [37], which comprises 22 able-bodied participants walking on a force-plate treadmill, each with 28 constant speed conditions distributed across 7 trials ranging from 0.5 to 1.85 m/s in 0.05 m/s increments, and 35 speed transition conditions. Speed transitions were periods of constant treadmill acceleration between different speed conditions, including accelerating

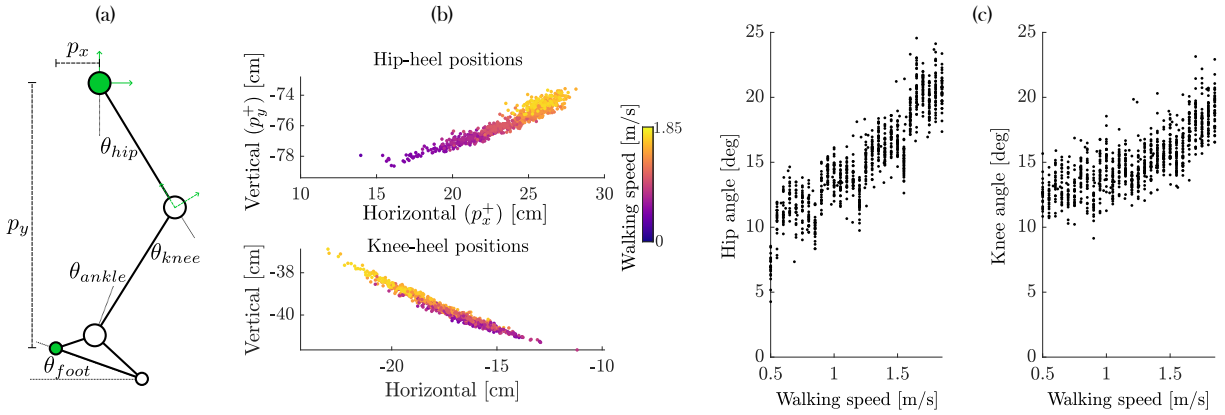

Fig. 2. (a) Simplified planar leg model defined by hip, knee, ankle, and global foot angles with global-oriented hip (solid green) and femur-oriented knee (dashed green) reference frames, and hip-heel positions p_x/p_y. (b) Right leg hip-heel positions in the hip frame and knee-heel positions in the knee frame. (c) Right hip and knee angles at right heel strike for all walking speeds for a single subject.

from 0 m/s and decelerating to 0 m/s at the start and end of each trial. Leg bone segment lengths for each subject were used to reconstruct a simplified planar leg model (Fig. 2a). Hip, knee, and ankle joint angles, and global foot angle, were applied to the leg model to derive the positions of the right heel relative to the right hip in the sagittal plane. Hip-heel velocity was calculated by differentiating hip-heel positions with respect to time. To capture both steady-state and non-steady-state walking, we included steps with and without treadmill speed changes between toe-off and heel-strike.

To construct the step placement model, let p and v represent the user's states — the instantaneous *sagittal* right hip-heel positions and velocities — and let the superscript indicate the moments of current $(-)$ and future $(+)$ heel strike. This model determines the predicted step placement states $\hat{p}^+$, and takes the following form:

$$\hat{p}_x^+ = \alpha_{x0} p_x^- + \alpha_{x1} v_x^- + \alpha_{x2}, \quad (1)$$

$$\hat{p}_y^+ = \alpha_{y0} p_y^- + \alpha_{y1} v_x^- + \alpha_{y2}, \quad (2)$$

where subscripts x/y indicate horizontal and vertical direction, respectively. We optimized scalar parameters α_{0-2} to minimize the error between the p^+ extracted from human data and the model output $\hat{p}^+ = f(p_{x/y}^-, v_x^-, \alpha)$ via a least squares minimization problem:

$$\alpha_{x/y} = \arg\min_{\alpha} \sum_{k=1}^{n} (\hat{p}_{x/y}^+(k) - p_{x/y}^+(k))^2, \quad (3)$$

considering a subject's n total step cycles across all trials. This process was performed separately for the x and y directions. We also developed a prediction model for the duration of swing phase, or single-support phase (SSP), denoted T_{SSP}, by constructing the following polynomial as a function of p_x^- and v_x^-,

$$\begin{aligned} \hat{T}_{SSP} = \beta_0 + \beta_1 p_x^- + \beta_2 v_x^- + \beta_3 p_x^- v_x^- \\ + \beta_4 \left(p_x^-\right)^2 + \beta_5 \left(v_x^-\right)^2, \end{aligned} \quad (4)$$

where the parameters β_{0-5} were optimized to fit $\hat{T}_{SSP}$ to T_{SSP}. The resulting complete step placement model provides user-desired values for $\hat{p}_{x/y}^+$ and $\hat{T}_{SSP}$ given user state measurements at the previous heel strike (Fig. 3a).

C. Swing Foot Trajectories

To bring the prosthesis foot to the desired step placement, we prescribe a trajectory to the prosthesis in swing phase. We defined trajectories for $p_{x/y}$ and the global foot angle, θ_{foot}, across the entire swing phase until $\hat{T}_{SSP}$. Importantly, we wanted the trajectory to resemble human foot movement across walking speeds to ensure smooth and natural motion, provide adequate ground clearance, and achieve heel strike. To accomplish this, we built normalized trajectories for each subject from averaged foot motion, which we de-normalize to generate a step-specific trajectory.

To construct these trajectories, we collected $p_{x/y}$ and θ_{foot} during each right leg swing phase for a given subject. Each resulting vector of different lengths was resampled to 100 data points. Vectors of $p_{x/y}$ were normalized by subtracting the first index value and dividing by the last index value. Vectors of θ_{foot} were normalized by dividing by the first index value. We then fit a 7th order Bézier polynomial to the average of each set of normalized vectors, such that the resulting polynomials progress along time-based phase variable $\tau \in [0\ 1]$.

Within our controller, a de-normalizing process is used to generate prosthesis trajectories based on the predictor model outputs $\hat{p}_{x/y}$ and $\hat{T}_{SSP}$. Each positional Bézier coefficient is first multiplied by the difference between the toe off and predicted heel strike hip-heel distances $(p^- - \hat{p}^+)$, then offset by adding $\hat{p}^+$. Bézier coefficients for θ_{foot} are multiplied by the initial θ_{foot} value since we do not predict the final value. We rescale τ to span $[0\,,\,\hat{T}_{SSP}]$ and evaluate the de-normalized coefficients to form continuous polynomial trajectories that progress from the toe-off value at time $t = 0$ to the final value at $t = \hat{T}_{SSP}$ (Fig. 3b). If heel strike does not occur by $t = \hat{T}_{SSP}$, the final trajectory values are gradually decreased to achieve ground contact.

D. Task-Space Control for Prosthesis Step Placement

Having created a model to predict desired step placement and constructed human-like trajectories to reach this step placement, we then formulated a tracking controller to enable the prosthesis to follow these trajectories. This task-space controller uses a rigid body dynamics model-based control

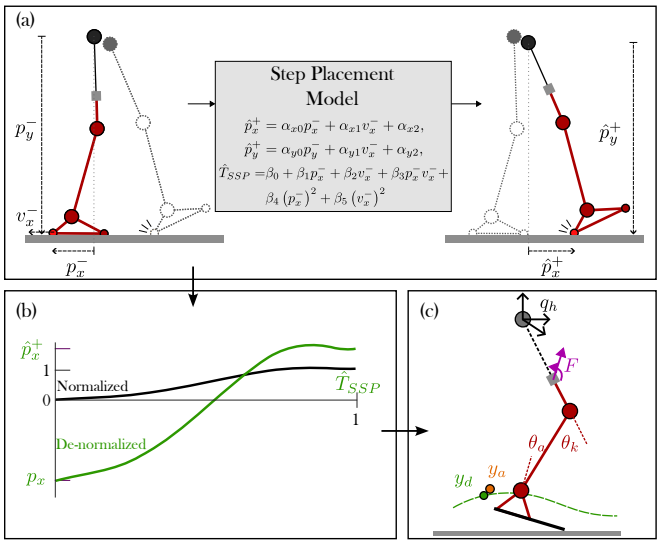

Fig. 3. (a) The step placement model predicts future prosthesis heel strike hip-heel positions and swing duration based on current heel strike stance states. (b) De-normalizing method for scaling Bézier coefficients for swing phase trajectory generation. (c) Prosthesis model with base coordinates q_h, knee coordinate θ_k, ankle coordinate θ_a, socket forces F, and output y_a (orange) tracking a desired trajectory y_d (green).

approach that considers the real-time dynamics of the user and the prosthesis.

A 3D three-link prosthesis model serves as the basis for designing task-space control for a transfemoral prosthesis user (Fig. 3c). We define the joint configuration $q = [q_h^T, q_p^T]^T \in \mathbb{R}^8$ as comprising six unactuated base coordinates $q_h \in \mathbb{R}^6$, representing the user's hip position and orientation, and two actuated prosthesis joints $q_p = [\theta_k, \theta_a]^T$, for the knee and ankle. The prosthesis socket is displaced from the base by the length of the residual femur, and the tibial pylon length is scaled such that the total leg length matches that of the corresponding human subject. Prosthesis component geometry, masses, and moments of inertia are defined by the MyoSim Open Source Leg (OSL) model [38] with the tibial pylon mass scaled by its new length. The Euler-Lagrange dynamics equation [39] for this system is:

$$D(q)\ddot{q} + H(q, \dot{q}) = Bu + J(q)^T F, \tag{5}$$

where $D(q)$ is the inertia matrix; $H(q, \dot{q})$ are gravitational, centrifugal, and Coriolis forces; $B = [0_{2\times 6}\ I_{2\times 2}]^T$ is the actuation matrix; u is the control input; and $J(q)$ is the Jacobian projecting the socket interaction forces and torques $F \in R^6$ into joint coordinates. We omit ground reaction forces from the model since swing phase does not include ground contact.

Task-Space Swing Control. Here, we formulate a model-based feedback-linearization controller to achieve continuous task-space trajectory tracking during swing phase using a method similar to [34], [40]. Let $y_a(q) = [p_x, p_y, \theta_{foot}]^T$ represent the prosthesis' planar hip-heel and foot angle values as a function of joint configuration $q \in \mathbb{R}^8$, and $y_d(\tau, b)$ represent the desired outputs defined by the de-normalized swing trajectory Bézier polynomials and phase variable τ. At time t, τ is evaluated as $\tau = \frac{t}{t_f - t_0}$, where t_0 is the start of swing phase and $t_f = \hat{T}_{SSP}$. We define the output of the task-space controller as $y = y_a - y_d$. To construct a control law that drives the output y to 0, we first differentiate $y(q)$ twice with respect to time, which yields output accelerations as functions of q and its derivatives:

$$\ddot{y}(q) = \frac{\partial}{\partial q}\left(\frac{\partial y}{\partial q}\dot{q}\right)\dot{q} + \frac{\partial y}{\partial q}\ddot{q}. \tag{6}$$

Solving (5) for $\ddot{q}$ and substituting this into (6) provides the mapping between heel acceleration and knee and ankle input torques u through Lie derivatives $L_f^2 y(q, \dot{q}) \in \mathbb{R}^3$ and $L_g L_f y(q, \dot{q}) \in \mathbb{R}^{3\times 2}$ [41]

$$\ddot{y}(q) = \underbrace{\frac{\partial}{\partial q}\left(\frac{\partial y}{\partial q}\dot{q}\right)\dot{q} + \frac{\partial y}{\partial q}\left(D(q)^{-1}(-H(q) + J^T F)\right)}_{L_f^2 y(q,\dot{q})} + \underbrace{\frac{\partial y}{\partial q}D(q)^{-1}B}_{L_g L_f y(q,\dot{q})}\, u. \tag{7}$$

To track the desired trajectory, we define an auxiliary feedback term $\mu = -K_P(y_a - y_d) - K_V(\dot{y}_a - \dot{y}_d)$ with tunable gains K_P and K_V. We compute the prosthesis torques u through:

$$u = L_g L_f y(q, \dot{q})^{-1}(-L_f^2 y(q, \dot{q}) + \mu + \ddot{y}_d). \tag{8}$$

The above is an over-constrained problem with 3 outputs and 2 inputs requiring a non-square matrix inversion of Lie derivative $L_g L_f y$. It also includes both translational and rotational outputs of varying importance for our step placement control. We therefore calculate $L_g L_f y^{-1}$ using a weighted damped Moore-Penrose pseudo-inverse: [42]:

$$L_g L_f y^{-1} = W_q J_W^T (J_W J_W^T + \lambda I)^{-1} W_x, \tag{9}$$

$$J_W = W_x\, L_g L_f y\, W_q, \tag{10}$$

where $W_q \in \mathbb{R}^2$ and $W_x \in \mathbb{R}^3$ are input and output weights, respectively, and λ is the damping coefficient. Values for K_P, K_V, W_x, and λ were tuned manually in the simulation environment described in III. The resulting u calculated by the task-space controller considers model dynamics and input/output weighting to track our desired trajectories during swing phase (Fig. 3c). Note that while the control output is defined via a planar model, the task-space controller realizes trajectory tracking with a 3D prosthesis model.

This control pipeline provides a general framework to develop user-specific step-placement prosthesis controllers. For a given user, a predictive step placement model and a normalized set of trajectories could be generated based on able-bodied data from a person with similar anthropomorphic parameters to the user. The task-space tracking controller accounts for real-time user dynamics through its inclusion of the interaction forces and hip states in the dynamic model. These measurements can be obtained via a socket-mounted six-axis load cell and inertia measurement unit (IMU) on a powered prosthesis platform [43]. While an IMU can only measure the rotational components of the hip states, the linear components can be set to 0 since they do not have a meaningful effect on the model dynamics. The feedback

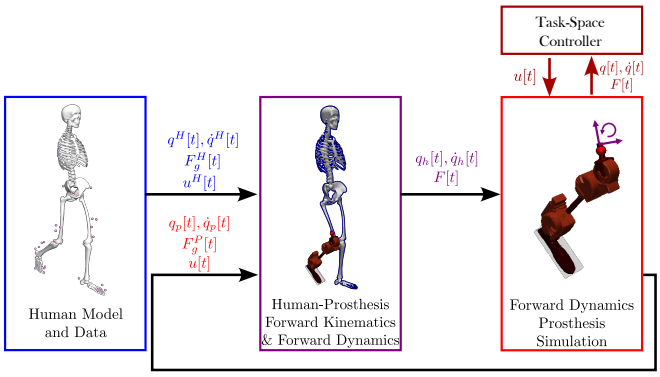

Fig. 4. Information flow between simulation environment components for swing phase task-space control. Human data provides inputs to a human-prosthesis model that determines the current human-prosthesis interaction, accounting for the current prosthesis dynamics. Based on the current human states and interaction forces, the prosthesis controller calculates new torque values and the prosthesis model dynamics are forward simulated.

linearizing controller can be realized on hardware through an inverse dynamics quadratic program, which provides a computationally feasible and numerically stable version of this control law [43], [44].

III. Human-Prosthesis Simulation

To test our step placement controller, we developed a novel human-prosthesis simulation environment that integrates human data with a forward dynamics prosthesis simulation to provide realistic human inputs and estimation of human-prosthesis interaction dynamics. We specifically used this simulation to evaluate the performance of our step placement control approach over a range of walking speeds.

Human-Prosthesis Model. The human-prosthesis model for the simulation consists of a 3D human skeleton spliced with a powered prosthetic leg (Fig. 4). We created MuJoCo skeletal models by converting the human models from [37] using the converter provided by [45]. We replaced the human leg segments distal to the right femur with the OSL model described in II-D. The OSL socket was attached to the right femur and positioned to match the hip-to-knee distance of the biological leg. Contact points were added to the bottom of the OSL foot.

During simulation, we prescribe positions, velocities, and torques (q^H, $\dot{q}^H$, u^H) from motion capture data [37] at time t to the human-prosthesis model's human joints. GRFs from force-plate data F_g^H are applied to the calcaneus of the sound limb. The prosthesis positions and velocities ($q_p, \dot{q_p}$), control torques u, and GRFs F_g^P come from a forward simulation of the prosthesis model. Based on this composition of pre-recorded human data and current prosthesis simulation data, the socket interaction forces F are determined through forward dynamics.

Prosthesis Forward Simulation. We perform a forward dynamics simulation on a separate prosthesis model to test our desired control. The global coordinates of the prosthesis model are set to the position of the prosthesis in the human-prosthesis model. The socket interaction forces determined from the human-prosthesis model are applied to the socket after being filtered with a first-order low-pass IIR filter to attenuate sudden socket force changes. GRFs are determined through a soft contact model at the foot contact points. The desired control inputs are applied to the prosthesis joints and then the prosthesis model is forward simulated for a single timestep via 4th-order Runge-Kutta integration. A constant time step of 10kHz is used to enhance simulation stability. These control inputs and the resulting joint positions, joint velocities, and GRFs are sent back to the human-prosthesis model to define the prosthesis kinematics and kinetics.

Step Placement Controller Simulations. In this simulation environment, we conducted extensive simulations of our prosthesis swing-phase step placement controller to assess its performance and ability to replicate the behavior of biological limbs. We defined a prosthesis heel reference point at the same location relative to the hip as the heel marker on the removed leg. This point was used to calculate $p_{x/y}$ and y_a. To determine our desired step placement, we calculated our inputs $p_{x/y}^-$ based on the human joint angles at left heel strike and a planar prosthesis model. For steps beginning from standing, the initial joint configuration was used. We then used human data at right toe off to set the initial conditions for the prosthesis simulation, and began forward simulation. Task-space control inputs were calculated at each time step and filtered with a first-order low-pass IIR filter to attenuate any sudden changes. In the control calculation, we set the Cartesian components of q_h and $\dot{q}_h$ to 0 since these quantities would be unknown on hardware. The simulation concluded once prosthesis heel strike occurred or $\hat{T}_{SSP} + 0.4s$ was reached. We performed simulations for 22 subject models, each with 28 steady-state and 35 non-steady-state walking conditions [37]. Each of these 1,386 walking conditions consisted of multiple steps, yielding a total of 20,571 swing phase simulations.

IV. Simulation Results

In this section we present the performance of our prosthesis step placement control approach. We evaluated predictive step placement model accuracy as the RMSE between the measured and predicted values for $p_{x/y}^+$ and T_{SSP}. Task-space controller performance was assessed by the tracking RMSE at $\hat{T}_{SSP}$. We assessed gait stability by the Margin of Stability (MoS) at heel strike. We calculated the RMSE between the MoS values from the human-prosthesis simulation and the human data of each step. All RMSE results were first computed per subject and then the mean across subjects was computed. Results are separated into means across all steps, only steady-state steps, and only non-steady-state steps. Results are plotted for subject AB12 from [37], who was chosen at random. The trends in controller performance for this subject are reflective of the trends seen across all subjects.

Predictive Step Placement Model Results. Our step placement model horizontal position, $\hat{p}_x^+$, predictions were, on average, within 1.9 cm of the ground truth hip-heel positions, p_x^+. This error slightly decreased for steady-state steps (1.5 cm), and was higher for non-steady-state steps (4.3 cm). The

TABLE I

STEP PLACEMENT PREDICTION ERROR ACROSS SUBJECTS

Prediction with Human Data Input $mean \pm s.d.$			
Step type	$\hat{p}_x^+$ [cm]	$\hat{p}_y^+$ [cm]	$\hat{T}_{SSP}$ [s]
All steps	1.9 ± 0.6	0.5 ± 0.1	0.032 ± 0.009
Steady-state	1.5 ± 0.5	0.4 ± 0.1	0.027 ± 0.008
Non-steady-state	4.3 ± 1.6	0.7 ± 0.2	0.066 ± 0.027
Prediction with Prosthesis Data Input $mean \pm s.d.$			
Step type	$\hat{p}_x^+$ [cm]	$\hat{p}_y^+$ [cm]	$\hat{T}_{SSP}$ [s]
All steps	1.9 ± 0.5	0.5 ± 0.1	0.033 ± 0.009
Steady-state	1.5 ± 0.5	0.4 ± 0.1	0.028 ± 0.008
Non-steady-state	4.3 ± 1.6	0.7 ± 0.2	0.066 ± 0.027

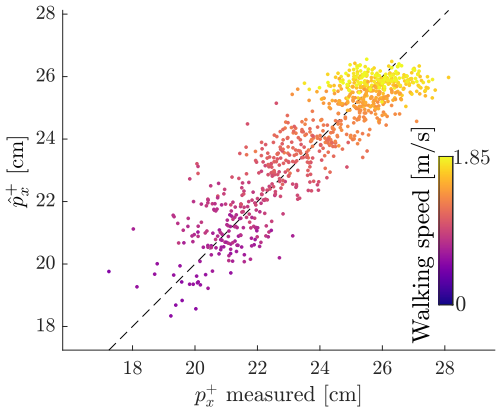

Fig. 5. Measured p_x^+ and predicted $\hat{p}_x^+$ for all steps for a single subject using human input data. Dashed line marks the ideal 1:1 relationship.

hip-heel positions predicted by the model compared to the ground truth for all walking speeds are shown for one subject in Fig. 5. The model achieved vertical hip-heel distance predictions, $\hat{p}_y^+$, and swing phase duration predictions, $\hat{T}_{SSP}$, within 0.5 cm and 0.032 s of the true values, on average. These errors were slightly smaller across steady-state steps, but increased for non-steady-state steps. All mean values and standard deviations are given in Table I.

Increased errors for non-steady-state steps are likely due to adjustments made by the subject during swing phase in response to ongoing treadmill speed changes. Since the predictive model does not update predictions during swing phase, these adjustments are not accounted for in the final prediction. Due to small segment length and joint orientation differences between the human limb and the prosthesis, predictions using the prosthesis model slightly changed the prediction errors, as shown in Table I. These results demonstrate the model's ability to capture subject-specific step placement patterns, thereby providing a systematic method to generate user-specific prosthesis controllers.

Task-Space Controller Results. Next, we present the task-space controller performance. Errors between the prosthesis foot and desired task-space trajectories throughout swing phase are depicted for all steps for a single subject (Fig. 6). Mean trajectory tracking RMSE at $\hat{T}_{SSP}$ is listed in Table II. These errors were on average 0.4 cm for the horizontal position, p_x, and 0.9 deg for the foot angle, θ_{foot}. Slightly smaller errors were seen in steady-state steps (0.3 cm, 0.7 deg) while higher errors were seen in non-steady-state steps

TABLE II

SWING TRAJECTORY TRACKING ERROR AT $\hat{T}_{SSP}$ ACROSS SUBJECTS

Tracking Error $mean \pm s.d.$			
Step type	p_x [cm]	p_y [cm]	θ_{foot} [deg]
All steps	0.4 ± 0.3	0.4 ± 0.1	0.9 ± 0.4
Steady-state	0.3 ± 0.1	0.4 ± 0.1	0.7 ± 0.2
Non-steady-state	1.0 ± 1.2	0.4 ± 0.2	1.6 ± 1.5

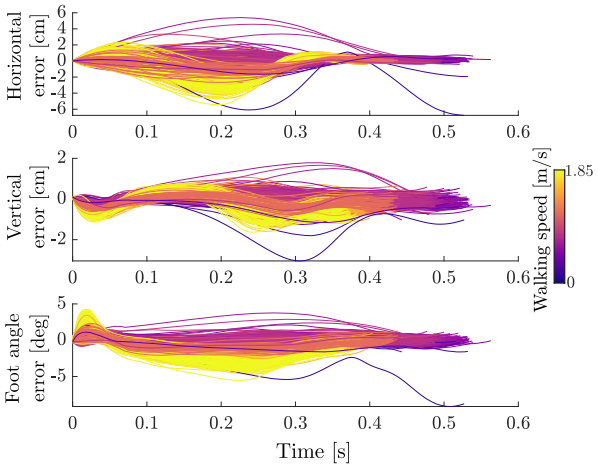

Fig. 6. Task-space controller tracking errors for horizontal/vertical heel position and foot angle for all steps for a single subject.

(1.0 cm, 1.6 deg). The increased errors at non-steady-state conditions is likely due to the higher error in step placement prediction at these conditions. This prediction error could have caused the trajectory to be more difficult to track, especially at the end of swing phase. However, vertical tracking error was much more consistent between steady-state and non-steady-state conditions (0.4 cm), suggesting this performance was less affected by the prediction errors at non-steady-state conditions.

One issue that arose was occasional heel or toe scuffs, where the heel or toe contact points went below the ground height well before $\hat{T}_{SSP}$. Heel strikes were considered heel scuffs if they occurred before $\hat{T}_{SSP} - 0.1$ s. Successful heel strikes without heel scuffing occurred in 98% of steps, and on average occurred 0.007 s after $\hat{T}_{SSP}$. Heel strikes did not occur in 0.005% of all steps. Heel and toe scuffs occurred in 2.0% and 0.3% of steps, respectively.

This tracking performance across 20,571 different trajectories highlights the ability of this model-based control approach to generalize across users and walking speeds. By only requiring updates to the physical prosthesis parameters while accounting for human dynamics through socket force and motion sensing, the controller adapts to various prothesis users and walking speeds without redesign.

Margin of Stability. MoS [29] is a widely-used biomechanical measurement of gait stability that considers the CoM position and velocity with respect to step placement. Specifically, it measures the relationship between the extrapolated CoM position and the anterior base of support (BoS) defined by the feet. In biomechanics research, sagittal plane MoS at heel strike is often used to assess how different walking conditions affect stability. While there is no discrete threshold

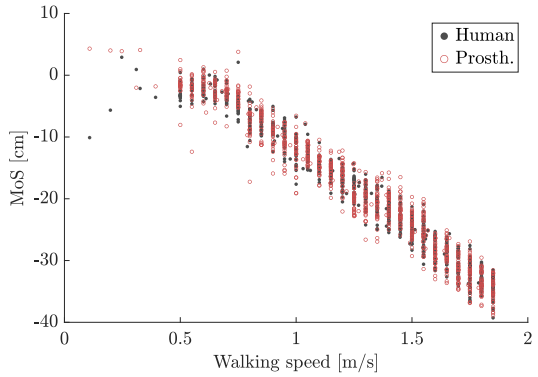

Fig. 7. Human and prosthesis right heel strike MoS values for all steps for a single subject.

that leads to falling, researchers use relative changes in the MoS to measure how subjects adjust their level of stability in response to walking conditions. For example, the MoS has been observed to decrease linearly with respect to walking speed [46]. The MoS is calculated as:

$$MoS = p_{BoS} - (p_{CoM} + \frac{v_{CoM}}{\omega_0}), \tag{11}$$

$$\omega_0 = \sqrt{g/L}, \quad g = 9.81\frac{m}{s^2}, \tag{12}$$

where p_{CoM} is the distance between the trailing foot and the CoM, p_{BoS} is the distance between the trailing foot and the front foot, v_{CoM} is the CoM velocity, g is gravitational acceleration, and L is the effective inverted pendulum length.

We assessed the performance of our prosthesis controller by comparing the MoS achieved by the human right leg and the prosthesis for the same steps. For both human and prosthesis MoS, we estimated the CoM position as the midpoint of the four sacroiliac markers on the pelvis filtered with a 4th-order Butterworth filter at 6 Hz. Differentiating the global CoM position yielded v_{CoM}. We measured L as the mean CoM height during a static standing trial. Human and prosthesis p_{BoS} were defined as the distance between the right foot/prosthesis heel marker and the left toe tip marker at human/prosthesis heel strike, respectively. With these values at the respective human or prosthesis heel strike, we calculated MoS and compared the quantities for steps that had a successful prosthesis heel strike.

Human and prosthesis MoS values are plotted against treadmill speed at heel strike for a single subject (Fig. 7). For all subjects, the human and prosthesis MoS follow similar downward trends to one another with respect to walking speed. Mean MoS RMSE across all subjects was 2.4 $\pm$ 1.1 cm for all steps, 2.3 $\pm$ 1.2 cm for steady-state steps, and 3.5 $\pm$ 1.3 cm for non-steady-state steps. The slightly higher MoS errors for non-steady-state steps is likely a result of the step placement prediction errors attributed to user adjustments during swing phase. Overall, these similar MoS patterns indicate that our prosthesis controller emulates human dynamic balance strategies, suggesting it may promote more stable and efficient gait and could reduce user compensatory behaviors.

V. Conclusion and Future Work

This work achieved human-like step placement behavior on a powered knee-ankle prosthesis in simulation. By constructing subject-specific step placement prediction models, we modulated swing-phase task-space trajectories to yield desired foot placement relative to the user's hip. This framework creates a unified objective for multi-joint prostheses, yielding a coordinated control approach that modulates the global quantity of step placement in response to whole-body states. Additionally, we developed a novel human-prosthesis 3D simulation environment that provides realistic human inputs and estimation of human-prosthesis interaction dynamics. Within this simulation, we assessed the performance of our step placement controller for 22 subject models and across a range of walking speeds and speed transitions. Our controller achieved human-like step-placement and gait stability patterns with respect to walking speed, as measured by Margin of Stability. These results demonstrate this control approach's potential to systematically generate user-specific controllers that enable stable, speed-adaptive prosthesis control, to support the daily activities of prosthesis users.

Future work will involve expanding the step placement predictor by developing a model of perturbed walking, enabling the prosthesis to react to more varied conditions and prevent falls. To improve our step placement predictions at non-steady-state walking, we will investigate methods to estimate the CoM online to update our step placement predictions during mid-swing. Additionally, we will consider incorporating a phase-variable into our trajectory generation to enable volitional control during swing-phase [13], [47]. The human-prosthesis model's physical realism can also be improved by adjusting the femur-socket interface constraint to model second-order interaction dynamics. Finally, incorporating speed-adaptive stance phase control would complete the framework to realize this controller on hardware and evaluate with people with amputation.

References

[1] J. A. Rivera, K. Churovich, A. B. Anderson, and B. K. Potter, "Estimating recent us limb loss prevalence and updating future projections," *Archives of Rehabilitation Research and Clinical Translation*, vol. 6, no. 4, p. 100376, 2024.

[2] M. S. Orendurff, J. A. Schoen, G. C. Bernatz, A. Segal, and G. K. Klute, "How humans walk: bout duration, steps per bout, and rest duration." *Journal of Rehabilitation Research & Development*, vol. 45, no. 7, 2008.

[3] M. P. Murray, R. C. Kory, B. H. Clarkson, and S. Sepic, "Comparison of free and fast speed walking patterns of normal men," *American Journal of Physical Medicine & Rehabilitation*, vol. 45, no. 1, pp. 8–24, 1966.

[4] J. A. Kent, J. H. Sommerfeld, M. Mukherjee, K. Z. Takahashi, and N. Stergiou, "Locomotor patterns change over time during walking on an uneven surface," *Journal of experimental biology*, vol. 222, no. 14, p. jeb202093, 2019.

[5] A. S. McIntosh, K. T. Beatty, L. N. Dwan, and D. R. Vickers, "Gait dynamics on an inclined walkway," *Journal of biomechanics*, vol. 39, no. 13, pp. 2491–2502, 2006.

[6] A. Kulkarni, C. Cui, S. Rietdyk, and S. Ambike, "Humans prioritize walking efficiency or walking stability based on environmental risk," *PLoS one*, vol. 18, no. 4, p. e0284278, 2023.

[7] M. van den Bogaart, S. M. Bruijn, J. H. van Dieën, and P. Meyns, "The effect of anteroposterior perturbations on the control of the center of mass during treadmill walking," *Journal of biomechanics*, vol. 103, p. 109660, 2020.

[8] M. Vlutters, E. H. Van Asseldonk, and H. Van der Kooij, "Center of mass velocity-based predictions in balance recovery following pelvis perturbations during human walking," *Journal of experimental biology*, vol. 219, no. 10, pp. 1514–1523, 2016.

[9] Y. Sagawa Jr, K. Turcot, S. Armand, A. Thevenon, N. Vuillerme, and E. Watelain, "Biomechanics and physiological parameters during gait in lower-limb amputees: a systematic review," *Gait & posture*, vol. 33, no. 4, pp. 511–526, 2011.

[10] A. K. Silverman and R. R. Neptune, "Three-dimensional knee joint contact forces during walking in unilateral transtibial amputees," *Journal of biomechanics*, vol. 47, no. 11, pp. 2556–2562, 2014.

[11] S. Farrokhi, B. Mazzone, S. Eskridge, K. Shannon, and O. T. Hill, "Incidence of overuse musculoskeletal injuries in military service members with traumatic lower limb amputation," *Archives of physical medicine and rehabilitation*, vol. 99, no. 2, pp. 348–354, 2018.

[12] R. Gehlhar, M. Tucker, A. J. Young, and A. D. Ames, "A review of current state-of-the-art control methods for lower-limb powered prostheses," *Annual reviews in control*, vol. 55, pp. 142–164, 2023.

[13] T. K. Best, C. G. Welker, E. J. Rouse, and R. D. Gregg, "Data-driven variable impedance control of a powered knee–ankle prosthesis for adaptive speed and incline walking," *IEEE Transactions on Robotics*, vol. 39, no. 3, pp. 2151–2169, 2023.

[14] D. Quintero, D. J. Villarreal, and R. D. Gregg, "Preliminary experiments with a unified controller for a powered knee-ankle prosthetic leg across walking speeds," in *2016 IEEE/RSJ International Conference on Intelligent Robots and Systems (IROS)*. IEEE, 2016, pp. 5427–5433.

[15] P. Sherpa and D. Quintero, "A unified control framework with continuous speed adaptation used for powered prostheses control," in *2021 International Symposium on Medical Robotics (ISMR)*, 2021, pp. 1–6.

[16] A. H. Shultz, B. E. Lawson, and M. Goldfarb, "Variable cadence walking and ground adaptive standing with a powered ankle prosthesis," *IEEE Transactions on Neural Systems and Rehabilitation Engineering*, vol. 24, no. 4, pp. 495–505, 2016.

[17] L. M. Sullivan, S. Creveling, M. Cowan, L. Gabert, and T. Lenzi, "Powered knee and ankle prosthesis control for adaptive ambulation at variable speeds, inclines, and uneven terrains," in *2023 IEEE/RSJ International Conference on Intelligent Robots and Systems (IROS)*. IEEE, 2023, pp. 2128–2133.

[18] J. Markowitz, P. Krishnaswamy, M. F. Eilenberg, K. Endo, C. Barnhart, and H. Herr, "Speed adaptation in a powered transtibial prosthesis controlled with a neuromuscular model," *Philosophical Transactions of the Royal Society B: Biological Sciences*, vol. 366, no. 1570, pp. 1621–1631, 2011.

[19] J. Mendez, S. Hood, A. Gunnel, and T. Lenzi, "Powered knee and ankle prosthesis with indirect volitional swing control enables level-ground walking and crossing over obstacles," *Science Robotics*, vol. 5, no. 44, p. eaba6635, 2020.

[20] T. Lenzi, L. Hargrove, and J. Sensinger, "Speed-adaptation mechanism: Robotic prostheses can actively regulate joint torque," *IEEE Robotics & Automation Magazine*, vol. 21, no. 4, pp. 94–107, 2014.

[21] N. Thatte, N. Srinivasan, and H. Geyer, "Real-time reactive trip avoidance for powered transfemoral prostheses." in *Robotics: Science and Systems*, 2019.

[22] D. J. Kelly and P. M. Wensing, "A task-space control framework for powered ankle prostheses: Design, implementation, and evaluation," *IEEE Transactions on Medical Robotics and Bionics*, 2025.

[23] S. M. O'Connor and A. D. Kuo, "Direction-dependent control of balance during walking and standing," *Journal of neurophysiology*, vol. 102, no. 3, pp. 1411–1419, 2009.

[24] S. M. Bruijn and J. H. Van Dieën, "Control of human gait stability through foot placement," *Journal of The Royal Society Interface*, vol. 15, no. 143, p. 20170816, 2018.

[25] P. E. Martin and A. P. Marsh, "Step length and frequency effects on ground reaction forces during walking," *Journal of biomechanics*, vol. 25, no. 10, pp. 1237–1239, 1992.

[26] Y. Wang and M. Srinivasan, "Stepping in the direction of the fall: the next foot placement can be predicted from current upper body state in steady-state walking," *Biology letters*, vol. 10, no. 9, p. 20140405, 2014.

[27] S. M. Bruijn, O. Meijer, P. Beek, and J. H. van Dieen, "Assessing the stability of human locomotion: a review of current measures," *Journal of the Royal Society Interface*, vol. 10, no. 83, p. 20120999, 2013.

[28] M. S. Redfern and T. Schumann, "A model of foot placement during gait," *Journal of biomechanics*, vol. 27, no. 11, pp. 1339–1346, 1994.

[29] A. L. Hof, "The 'extrapolated center of mass' concept suggests a simple control of balance in walking," *Human movement science*, vol. 27, no. 1, pp. 112–125, 2008.

[30] D. Joshi, A. Mishra, and S. Anand, "Anfis based knee angle prediction: An approach to design speed adaptive contra lateral controlled ak prosthesis," *Applied Soft Computing*, vol. 11, no. 8, pp. 4757–4765, 2011.

[31] J. Pratt, J. Carff, S. Drakunov, and A. Goswami, "Capture point: A step toward humanoid push recovery," in *2006 6th IEEE-RAS international conference on humanoid robots*. Ieee, 2006, pp. 200–207.

[32] X. Xiong and A. Ames, "3-d underactuated bipedal walking via h-lip based gait synthesis and stepping stabilization," *IEEE Transactions on Robotics*, vol. 38, no. 4, pp. 2405–2425, 2022.

[33] J. Camargo, K. Bhakta, and A. Young, "Stochastic optimization of impedance parameters for a powered prosthesis using a 3d simulation environment," in *Dynamic Systems and Control Conference*, vol. 51913. American Society of Mechanical Engineers, 2018, p. V003T29A006.

[34] R. Gehlhar, "Model-based lower-limb powered prosthesis control: Developing and realizing nonlinear subsystem control methods for generalizable prosthesis control," Ph.D. dissertation, California Institute of Technology, 2023.

[35] R. Gehlhar, Y. Chen, and A. D. Ames, "Data-driven characterization of human interaction for model-based control of powered prostheses," in *2020 IEEE/RSJ international conference on intelligent robots and systems (IROS)*. IEEE, 2020, pp. 4126–4133.

[36] X. Xiong, Y. Chen, and A. D. Ames, "Robust disturbance rejection for robotic bipedal walking: System-level-synthesis with step-to-step dynamics approximation," in *2021 60th IEEE Conference on Decision and Control (CDC)*. IEEE, 2021, pp. 697–704.

[37] J. Camargo, A. Ramanathan, W. Flanagan, and A. Young, "A comprehensive, open-source dataset of lower limb biomechanics in multiple conditions of stairs, ramps, and level-ground ambulation and transitions," *Journal of Biomechanics*, vol. 119, p. 110320, 2021.

[38] C. Vittorio, W. Huawei, D. Guillaume, S. Massimo, and K. Vikash, "Myosuite – a contact-rich simulation suite for musculoskeletal motor control," https://github.com/facebookresearch/myosuite, 2022.

[39] R. M. Murray, S. S. Sastry, and L. Zexiang, *A Mathematical Introduction to Robotic Manipulation*, 1st ed. Boca Raton, FL, USA: CRC Press, Inc., 1994.

[40] A. E. Martin and R. D. Gregg, "Hybrid invariance and stability of a feedback linearizing controller for powered prostheses," in *2015 American Control Conference (ACC)*, 2015, pp. 4670–4676.

[41] A. Isidori, *Nonlinear control systems: an introduction*. Springer, 1985.

[42] D. Schinstock, T. Faddis, and R. Greenway, "Robust inverse kinematics using damped least squares with dynamic weighting," in *NASA. Johnson Space Center, Conference on Intelligent Robotics in Field, Factory, Service and Space (CIRFFSS 1994), Volume 2*, no. AIAA PAPER 94-1299-CP, 1994.

[43] R. Gehlhar and A. D. Ames, "Emulating human kinematic behavior on lower-limb prostheses via multi-contact models and force-based nonlinear control," in *2023 IEEE International Conference on Robotics and Automation (ICRA)*, 2023, pp. 10 429–10 435.

[44] J. Reher, C. Kann, and A. D. Ames, "An inverse dynamics approach to control lyapunov functions," in *2020 American Control Conference (ACC)*. IEEE, 2020, pp. 2444–2451.

[45] A. Ikkala and P. Hämäläinen, "Converting biomechanical models from opensim to mujoco," in *Converging Clinical and Engineering Research on Neurorehabilitation IV: Proceedings of the 5th International Conference on Neurorehabilitation (ICNR2020), October 13–16, 2020*. Springer, 2022, pp. 277–281.

[46] C. McCrum, P. Willems, K. Karamanidis, and K. Meijer, "Stability-normalised walking speed: a new approach for human gait perturbation research," *Journal of biomechanics*, vol. 87, pp. 48–53, 2019.

[47] K. R. Embry, D. J. Villarreal, R. L. Macaluso, and R. D. Gregg, "Modeling the kinematics of human locomotion over continuously varying speeds and inclines," *IEEE transactions on neural systems and rehabilitation engineering*, vol. 26, no. 12, pp. 2342–2350, 2018.